Journal of Translational Medicine

RESEARCH

Open Access

RBM15 recruits myeloid-derived suppressor cells via the m6A-IGF2BP3/CBR3-AS1/miR-409-3p/CXCL1 axis, facilitating radioresistance in non-small-cell lung cancer

Songliu Hu[1†], Ning Zhan[2†], Jian Li[1†], Liqun Wang[1], Yiyan Liu[3], Ke Jin[1], Yixuan Wang[1], Juxuan Zhang[3], Yiyang Chen[1], Yang Bai[1], Yichong Wang[1], Lishuang Qi[3*] and Shilong Liu[1*]

Abstract

Background Radiotherapy is commonly used for locoregionally advanced NSCLC, but radioresistance is a clinical challenge. The long non-coding RNA CBR3-AS1 mediates radioresistance in NSCLC, yet the underlying molecular mechanism is unclear. This study aims to explore whether and how N6-methyladenosine (m6A) modification regulates CBR3-AS1 expression and promotes NSCLC radioresistance.

Methods Integrative bioinformatics analyses were used to investigate the m6A methyltransferases that were associated with CBR3-AS1 expression and radioresistance of patients using data from The Cancer Genome Atlas of lung adenocarcinoma and squamous cell carcinoma. Clinical samples of 133 patients with NSCLC was collected to validate the correlation of the methyltransferase with radioresistance. The functional role and molecular mechanism of the methyltransferase in radioresistance was investigated through a series of in vitro experiments including m6A MeRIP-PCR, lentivirus transfection, RNA immunoprecipitation, Luciferase reporter, Colony formation, Transwell invasion, Flow cytometry, ELISA and TUNEL assay and in vivo experiments.

Results The methyltransferase RNA binding motif protein 15 (RBM15) was identified as it was significantly positively correlated with CBR3-AS1 expression and overall survival of NSCLC patients receiving radiotherapy. The clinical samples demonstrated that the high protein expression of RBM15 was significantly enriched in patients with radioresistance as well as associated with poor prognosis of patients receiving radiotherapy. In vitro, RBM15 silencing enhanced the effects of radiation on the growth and invasion inhibition, and apoptosis induction of NSCLC cells; RBM15 overexpression had the opposite effects. Mechanistically, RBM15 induced CBR3-AS1 upregulation via an m6A-IGF2BP3-dependent mechanism, inducing CXCL1 expression by sponging miR-409-3p to recruit myeloid-derived suppressor cells (MDSCs) and inhibit T cell activity. In vivo, RBM15 silencing suppressed MDSC invasiveness and enhanced CD8 + and CD4 + T cell infiltration, causing NSCLC cells to overcome radioresistance.

[†]Songliu Hu, Ning Zhan and Jian Li have contributed equally to this work.

*Correspondence:
Lishuang Qi
qilishuang7@ems.hrbmu.edu.cn
Shilong Liu
liushilong1984@hrbmu.edu.cn
Full list of author information is available at the end of the article

Conclusion Our study identifies methyltransferase RBM15 as a potential therapeutic target for NSCLC radioresistance whose inhibition reverses resistance through limiting MDSC recruitment via the m6A-IGF2BP3-CBR3-AS1/miR-409-3p/CXCL1 axis.

Highlights

- RBM15 induces CBR3-AS1 via an m6A-IGF2BP3 mechanism, promoting NSCLC radioresistance.
- CBR3-AS1 induces CXCL1 by sponging miR-409-3p to recruit MDSCs and inhibit T cells.
- RBM15 is a radiosensitization target for NSCLC as the RBM15 depletion reverses the radioresistance.

Keywords lncRNA CBR3-AS1, RBM15, m6A modification, MDSCs, Non-small-cell lung cancer, Radioresistance

Graphical Abstract

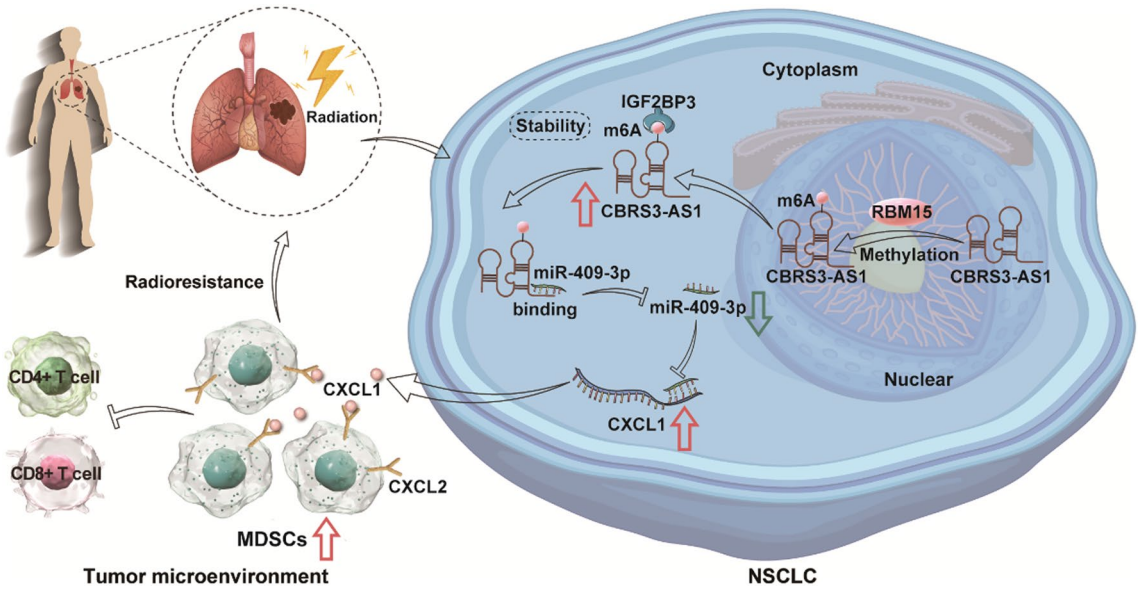

Background

Lung cancer is the most common cause of cancer-related deaths worldwide. It is estimated that by 2024, there will be 234,580 newly diagnosed cases of lung cancer and 125,070 deaths attributable to lung cancer [1]. Non-small-cell lung cancer (NSCLC) accounts for approximately 80% of primary lung cancers [2], and approximately 50% of patients present with locoregionally advanced stages at first diagnosis [1]. Radiotherapy is used to treat 50–60% of patients with NSCLC [3]. Despite continuous technological and therapeutic improvements, radioresistance remains a major issue that limits the clinical efficacy and prognosis of patients with NSCLC. Therefore, there is an urgent need to uncover the potential mechanisms underlying radioresistance and develop radiosensitizing strategies to improve the prognosis of patients with NSCLC.

Our previous study reported that the long non-coding RNA (lncRNA) CBR3-AS1 participates in the oncogenesis and radioresistance of NSCLC by regulating miR-409-3p as a sponge [4]. Several studies have also demonstrated that CBR3-AS1 functions as an oncogene in multiple cancers [5–7]. Nevertheless, further research is required to elucidate the complex molecular mechanisms underlying the role of CBR3-AS1 in radioresistance.

N6-methyladenosine (m^6A) is the most common epigenetic modification in RNA. m^6A modifications regulate the splicing, translation, and decay rates of RNA, thereby affecting several biological processes [8, 9]. This modification is mediated by m^6A methyltransferases (m^6A "writers"), including METTL3/14, WTAP, and RBM15, and can be removed by demethylases (m^6A "erasers"),

such as FTO11 and ALKBH5 [10]. The functional effects of m^{6}A on RNA metabolism and translation are mediated through m^{6}A "readers", including YTHDF1/2, YTHDC1/2/3, and IGF2BP1/2/3 [11, 12]. Several studies have shown that aberrant m^{6}A modifications play a crucial role in the development and treatment of various cancers [12, 13]. Therefore, exploring whether and how m^{6}A modification regulates CBR3-AS1 overexpression and its significance in the response of tumor cells to radiotherapy will help identify novel targets to alleviate or overcome radioresistance.

Accumulating evidence indicates that radiotherapy failure is closely related to the tumor microenvironment (TME). Myeloid-derived suppressor cells (MDSCs), the primary suppressive cells within the TME, are characterized by their ability to suppress T cell proliferation and function, allowing tumor cells to escape immune attack and promote their resistance to radiotherapy [14]. It has been suggested that MDSC accumulation mainly results from the recruitment of cytokines secreted by tumor cells [9–11]. Previous studies have found that C-X-C motif chemokine ligand 1 (CXCL1) is a target of miR-409-3p, which plays a vital role in recruiting MDSCs into the tumor tissue [15]. However, the association between CBR3-AS1/miR-409-3p and MDSC accumulation in NSCLC remains unclear.

In the present study, bioinformatics analyses revealed that m^{6}A was highly enriched within CBR3-AS1 and that the methyltransferase RBM15 induced CBR3-AS1 expression in an m^{6}A-dependent manner, promoting radioresistance in NSCLC. Clinical samples and in vitro experiments validated the association between RBM15 and radioresistance of NSCLC. Mechanistically, the m^{6}A reader IGF2BP3 was identified, which was bound to m^{6}A-modified CBR3-AS1 to facilitate its stability and overexpression. CBR3-AS1 overexpression constantly induced CXCL1 expression by sponging miR-409-3p, which enhanced its binding to CXCR2. This binding recruits MDSCs and inhibits T cell activity, eventually promoting NSCLC radioresistance in vitro and in vivo. In general, our findings shed light on a new mechanism of radioresistance in NSCLC via the m^{6}A- IGF2BP3/CBR3-AS1/miR-409-3p/CXCL1 axis mediated by RBM15, suggesting a novel therapeutic strategy against radioresistance in patients with NSCLC.

Methods

Public data sources and preprocessing

RNA sequencing (RNA-seq) data of lung adenocarcinoma (LUAD), lung squamous carcinoma (LUSC) and normal controls were downloaded from The Cancer Genome Atlas (TCGA, http://cancergenome.nih.gov/). Based on the clinical information, we selected 107 LUAD and 71 SCC patients who received radiotherapy and 109 normal controls. The fragments per kilobase of transcript per million (FPKM) mapped read values for the RNA-seq data generated using the Illumina HiSeq 2000 platform were log2-scaled plus 1 and then processed using the Combat method (R package "SVA") to correct the batch effects between TCGA-LUAD and TCGA-LUSC datasets.

Tissue samples and immunohistochemistry (IHC)

We obtained 133 tissue specimens from NSCLC patients at the Affiliated Tumor Hospital of Harbin Medical University between June 2009 and January 2020. The eligible patients met the following criteria: pathologically confirmed NSCLC, unresectable stage IIb–IIIc, receiving radical radiotherapy with or without chemotherapy, no anti-tumor therapy before radiotherapy, and recording complete prognostic follow-up information. The patients' chest computed tomography scans were reviewed one month after radiotherapy, and according to the criteria for evaluating the efficacy of solid tumors (RECIST 1.1), 3 complete response (CR) and 71 partial response (PR) patients were classified as radiosensitive, and 42 stable disease (SD) and 17 progressive disease (PD) patients were classified as radioresistant. This study was approved by the Ethics Committee of Harbin Medical University Cancer Hospital (KY2022-57), and written consent was provided by patients or relatives before participating in this study.

Tissue sections were processed using standard deparaffinization, rehydration, antigen retrieval, and hydrogen peroxide treatments. Sections were incubated with anti-RBM15 primary antibodies (1:100, Abclonal, USA, A4936) at 4 °C overnight, followed by biotin-labeled secondary antibodies (1:500, thermoFisher, USA, #31460) and HRP-conjugated avidin. Staining was performed with DAB and hematoxylin. Two independent, blinded pathologists evaluated staining intensity and proportion of positive cells, staining scoring from 0 to 7. Specimens with scores ≥ 5 were classified as high RBM15 expression.

Cell culture and transfection

NSCLC cell lines (A549, H1650, H520, H460, H1299, PC9) and bronchial epithelial cells (BEAS-2B) were cultured in DMEM or RPMI-1640 with 10% FBS at 37 °C, 5% CO_2. Cells were transfected with RBM15, IGF2BP3, CBR3-AS1, miR-409-3p, CXCL1 or shRNA using lentiviruses (GeneChem, Shanghai, China) per the manufacturer's instructions. Stable cell lines were selected using

puromycin (3 μg/mL). Detailed sequences are in Supplementary Table S1.

Real-time PCR

The real-time PCR protocol utilized in this study was described in detail in a previous study [16]. Total RNA was extracted using TRIpure (BioTeke, Beijing, China, RP1001). cDNA was synthesized using the BeyoRT II M-MLV reverse transcriptase (Beyotime, Jiangsu, China, D7160L), and qRT-PCR was performed using a Fast Start Universal SYBR Green Master (ROX) (Solarbio, Beijing, China, SY1020) on an ABI7500 system according to the manufacturer's instructions. The data were analyzed via RT-qPCR using β-actin as the internal control. Primer details are provided in Supplementary Table S2. The fold-change in gene expression levels was calculated using the $2^{-\Delta\Delta Ct}$ method.

Western blotting

The western blotting protocol utilized in this study has also been described in detail in a previous study [16]. Proteins were extracted using a Whole Protein Extraction Kit (Wanleibio, Shenyang, China, WLA019). Membranes were probed with primary antibodies: RBM15 (1:500, Abclonal, USA, A4936), IGF2BP3 (1:1000, Abclonal, A4444), CXCL1 (1:500, Abclonal, USA, A5802), CXCR2 (1:1000, Proteintech, Wuhan, China, 20634-1-AP), or β-actin (1:500, Abclonal, USA, WL01372). Protein bands were developed using enhanced chemiluminescence (Wanleibio, Shenyang, China, WLA003), and quantified with Gel image processing system (Gel-Pro-Analyzer software).

m^6A RIP (MeRIP)-qPCR assay

m^6A methylation was quantified using an m^6A RNA methylation quantification kit (Ribobio, Guangzhou, China, R11096.4). The RNA was purified and fragmented, and was separated into 1/10 as the input group, others were incubated with anti-m6A primary antibodies for immunoprecipitation using m6A RNA methylation quantification kit (Ribobio, Guangzhou, China, R11096.4). Enriched m^6A-modified RNA was then analyzed using real-time PCR.

RNA immunoprecipitation (RIP) assay

RIP assays used the EZ-Magna RIP kit (Millipore, USA, 17–701) according to the operating instructions. Briefly, H520 cell were harvested and lysed on ice with RIP lysate, then the lysates were incubated with magnetic beads conjugated with anti-IGF2BP3 (Abclonal, USA, A4444) or control IgG (Beyotime, Shanghai, China, A7001) for immunoprecipitation. RNA was extracted after antigen capture and analyzed via real-time PCR.

Luciferase reporter assay

Luciferase assays were performed using a dual-luciferase reporter assay system (KeyGEN BioTECH, Jiangsu, China, KGAF040) according to the manufacturer's instructions. Briefly, plasmids containing either wild-type or mutant sequences were cloned into a pmirGLO reporter vector. Details regarding the DNA sequences are shown in Supplementary Table S3. The plasmids were verified via DNA sequencing. Cells were seeded in 12-well plates and transfected with luciferase vectors using Lipofectamine 3000 (Invitrogen, USA, L3000015). Three wells in a 12-well plate as one group: siRNA dosage: 45 pmol; Plasmid DNA amount: 1.5 μg. After 48 h, the firefly and *Renilla* luciferase activities in each well were assessed.

Cell counting Kit-8 (CCK8) assay

Cell proliferation was assessed using a CCK-8 kit (Wanleibio, Shenyang, WLA074) following the manufacturer's instructions. Briefly, cells were seeded in 96-well plates at a density of 2×10^3 cells per well and incubated at 37 °C in a 5% CO_2 incubator for 24, 48, 72, or 96 h. At the specified time points, 10 μl of CCK-8 solution was added to each well and incubated for 2 h. Absorbance at 450 nm was then measured using a microplate reader (BIOTEK, Vermont, USA, 800TS). Cell proliferation curves were plotted based on the absorbance values (OD = 450 nm) at each time point. Each sample was tested in five replicate wells, and the experiment was performed in triplicate.

Colony formation assay

Cells (300/well) were cultured in 6-well plates for 2 weeks. When clones were grossly visible, Paraformaldehyde was added to fixed and stained with Giemsa dye, and counted. Clones of more than 50 cells were counted under microscopy. Clone formation efficiency was tallied using the following formulas:

$$\text{Clone Formation Efficiency} = \left(\frac{\text{Number of Clones Formed}}{\text{Number of Inoculated Cells}}\right) \times 100\%$$

Transwell invasion assay

Transwell inserts (LABSELECT, Anhui, China, 14341) were coated with Matrigel (Corning, NY, USA). Cell suspensions were added to the upper chamber, with medium containing 10% FBS in the lower chamber. After 24–48 h, cells that migrated were stained with crystal violet and counted using an inverted microscope.

MDSCs were isolated from the spleens of C57BL/6 mice referring to previous research [17], sorted by flow-through to identify CD11b + Gr-1 + MDSCs. Herein, MDSCs (1×10^5 cells/well) were seeded in the top chamber of a Transwell (pore size: 8 μm) in 100 μL RPMI medium containing 10 ng/mL granulocyte–macrophage colony-stimulating factor (GenScript, Nanjing, China, Z03300) and interleukin (IL)-4 (SinoBiological, Beijing, China, 51084-MNAE). The bottom chamber contained 600 μL conditioned medium (without FBS) containing H520 cells or the CXCR2 antagonist SB265610 (Aladdin, Shanghai, China, S288762). After incubation for 24 h, the cells that migrated to the bottom chamber were counted.

Wound healing assay

H520 cells were seeded in 6-well culture plates. After monolayer formation, a scratch was made using a 200μL pipette tip. Cells were washed with PBS and incubated in serum-free medium. Images were captured at 0, 24, and 48 h using a microscope (Olympus IX53). Image J software was used for data analysis.

Flow cytometry

Apoptosis was analyzed using an Annexin V-FITC/PI Kit (Wanleibio, Shenyang, China, WLA001) with a NovoCyte flow cytometer (Agilent, California, USA, NovoCyte). The protocol has also been described in detail in a previous study [16]. Briefly, tumor tissues were digested with collagenase D (Merck, USA, 11088858001), filtered, and centrifuged. Single-cell suspensions were then prepared. Antibodies against mouse Ly-6G (Gr-1) (Lianke Bio, China, F21LY6G01), human/mouse CD11b PE (Lianke Bio, F11011B02), mouse CD4 PE (Proteintech, PE-65104), mouse IFN-γ APC (Lianke Bio, F21IFNG03), and mouse CD8α, FITC (LiankeBio, Hangzhou, China, F2100801) were used. Data were analyzed using FlowJo software.

Enzyme linked immunosorbent assay (ELISA)

Mouse IFN-γ levels were measured using an ELISA Kit (LiankeBio, Hangzhou, China, EK280) to assess the inhibitory effect of MDSCs on $CD4^+$ and $CD8^+$ T cells. T cells were activated with CD3/CD28 Dynabeads (T cell:beads = 2:1; Thermo Fisher Scientific, MA, USA, 11456D) and IL-4 (30 U/mL; Sino Biological, Beijing, China, 51084-MNAE), and monensin (Aladdin, Shanghai, China, M118287) was added 5 h before the end of the experiment to inhibit cytokine secretion.

Animal models

Male C57BL/6 mice (5–6 weeks, 20–25 g) were obtained from Vital River Laboratories. All procedures complied with Harbin Medical University's animal care guidelines (JJZD 2023-01). Mice were injected with lentivirus-transfected tumor cells (4×10^6 cells/200 μL). When tumors reached ~ 200 mm^3, mice were divided into four groups and treated with localized radiation (4 Gy) or sham treatment every 3 days for a total of five sessions. Tumor volumes were measured every 3 days. Animals were euthanized 3 days after the last radiotherapy session. Tumor histology was examined using HE staining.

TUNEL assay

Apoptosis was assessed using a TUNEL assay kit (Wanleibio, Shenyang, China, WLA030a). Tumor tissues were fixed in 4% paraformaldehyde for 48 h, rinsed with tap water for 4 h, and dehydrated with alcohol (70%, 80%, 90%, 100%). The tissues were embedded in dimethylbenzene and paraffin, and then were cut into 5 μm slices and fixed on each slide. Then, we baked the slices in an incubator at 60℃ for 4 h and set aside for later use. After the slices were dewaxed with dimethylbenzene, absolute ethanol (95%, 85%, 75%) in turn, we used the TUNEL assay kit to permeabilize, label and fluorescently stain the slides according to the instructions. Finally, the samples were sealed with anti-fluorescence quenched seal and observed by a fluorescence microscope in a dark environment and photographed.

Statistical analyses

Pearson correlation was used to estimate gene expression correlations. Differences between groups were assessed using Student's t-test or one-way ANOVA. Fisher's exact test evaluated differences in proportions.

Overall survival (OS) was defined as the time from diagnosis to death or last contact. Progression-free survival (PFS) was defined as the time from diagnosis to disease progression or death. Survival curves were estimated using the Kaplan–Meier method and compared with the log-rank test. Hazard ratios (HRs) and 95% confidence intervals (CI) were calculated using univariate Cox proportional-hazards models.

Data were expressed as mean ± standard deviation (SD) from at least three independent experiments. Analyses were conducted using R software version 4.3.2 or GraphPad Prism 9.5. *P* values were adjusted using the Benjamini–Hochberg procedure for multiple tests to control false discovery rate (FDR). Differences with two-sided $P < 0.05$ or FDR < 0.05 were considered statistically significant.

Results

RBM15 mediates the m^{6}A modification of CBR3-AS1 and facilitates radioresistance in NSCLC

To explore the m^{6}A modification of the lncRNA CBR3-AS1, we first used the online tool SRAMP (http://

www.cuilab.cn/sramp) to predict m^{6}A modification sites on CBR3-AS1. We identified three CBR3-AS1 sequence motifs with very high confidence (Fig. 1A, B). We then collected 11 methyltransferases, including *METTL3, METTL14, METTL16, METTL5, WTAP, VIRMA, RBM15, RBM15B, ZC3H13, CBLL1* and *ZCCHC* [18–21], and estimated the correlations of 11 methyltransferases with the expression of CBR3-AS1, carcinogenesis, and survival in an integrated transcriptomic profile of TCGA-LUAD and TCGA-LUSC. Ultimately, RBM15 was selected as it was significantly associated with the CBR3-AS1 expression (Pearson correlation, $P = 0.0063$, r = 0.20; Fig. 1C), upregulated in NSCLC (Wilcoxon rank-sum test, $P < 0.0001$; Fig. 1D), and was associated with the OS of patients receiving radiotherapy (high expression vs. low expression, log-rank $P = 0.0040$, HR = 1.85, 95% CI 1.21–2.83; Fig. 1E). Furthermore, we performed molecular docking of RBM15 with the three m^{6}A site sequence motifs (very high confidence) of CBR3-AS1 and found that RBM15 had excellent docking activity to CBR3-AS1 (binding energy < −8.0 kcal/mol; Fig. 1F). Finally, we collected 133 NSCLC specimens to confirm the association between RBM15 protein expression and radioresistance in patients with NSCLC. The clinicopathological characteristics of the patients and their associations with RBM15 expression are presented in Table 1. Representative immunohistochemical staining photographs of RBM15 protein expression in radioresistant and radiosensitive samples are shown in Fig. 1G. The staining scores of RBM15 were significantly higher in the 61 radioresistant samples than in the 72 radiosensitive samples (Wilcoxon rank-sum test, $P < 0.0001$; Fig. 1H). Moreover, 85.24% of the radioresistant samples were classified into the high-RBM15 group (score ≥ 5), significantly higher than the proportion (40.38%) of radiosensitive samples classified into the high-RBM15 group (Fisher's exact test, $P < 0.0001$; Fig. 1I). Survival analysis validated that the 81 patients in the high-RBM15 group had significantly shorter OS and PFS than the 52 low-RBM15 patients (OS: log-rank $P < 0.001$, HR = 2.29, 95% CI 1.54–3.42, Fig. 1J; PFS: log-rank $P = 0.041$, HR = 1.56, 95% CI 1.02–2.38, Fig. 1K).

RBM15 promotes NSCLC radioresistance through IGF2BP3-mediated CBR3-AS1 stabilization

We detected the mRNA and protein expression levels of RBM15 in six NSCLC cell lines (A549, H1650, H520, H460, H1299, and PC9) and bronchial epithelial cells (BEAS-2B), and found that RBM15 were significantly higher in six NSCLC cell lines than that in BEAS-2B ($P < 0.05$, Fig. 2A, B). As expected, the expression of CBR3-AS1 was also the highest in H520 cells (Fig. 2C). To investigate the role of RBM15 in NSCLC, we established stable H520-RBM15 and H520-shRBM15 cells and the corresponding control H520 cells (vecCtrl and shCtrl). Radiation treatment (8 Gy) was administered to all four transfected cell groups after 24 h. The effectiveness of stable genetic transfer was validated via PCR and western blotting (Supplementary Fig. S1A and S1B).

To clarify the effect of RBM15 on CBR3-AS1 m^{6}A modification in NSCLC, we first performed m^{6}A quantification assays. We found a significant increase in global m^{6}A levels in the RBM15 group compared to the empty vector control (vecCtrl) group and a significant reduction in global m^{6}A levels in the shRBM15 group compared with those in the shCtrl group (Fig. 2D). MeRIP-qPCR analysis showed that RBM15 overexpression significantly increased the m^{6}A modification level of CBR3-AS1 (Fig. 2E), accompanied by a considerable increase in CBR3-AS1 expression (Fig. 2F). RBM15 silencing significantly decreased the level of m^{6}A modification and CBR3-AS1 expression (Fig. 2E, F). Next, we treated H520 cells with the transcription inhibitor actinomycin D (ActD) and compared the half-life of CBR3-AS1 between the RBM15 or shRBM15 groups with the

(See figure on next page.)

Fig. 1 Bioinformatics analyses reveal that RBM15 is a potential methyltransferase of the lncRNA CBR3-AS1 and is involved in radioresistance in patients with NSCLC. **A** Enriched and specific m^{6}A peak distribution of CBR3-AS1 transcripts was predicted using the online SRAMP tool. The red arrows indicate m^{6}A modification sites with very high confidence in the m^{6}A enrichment peaks at nucleotide positions 448–532 of the lncRNA CBR3-AS1 transcripts. **B** Diagram showing the position of m^{6}A motifs with very high confidence within the CBR3-AS1 transcripts. **C** Correlation between methyltransferase and CBR3-AS1 expression estimated by Pearson correlation analysis. **D** Box plot of RBM15 expression in patients with NSCLC and normal controls. The difference was estimated by Wilcoxon rank-sum test. **E** Kaplan–Meier survival curves of patients with NSCLC who received radiotherapy stratified by RBM15 mRNA expression in TCGA-NSCLC cohort. The OS difference was estimated by log-rank test, and HR and 95% CIs were calculated using univariate Cox model. **F** Interaction probabilities of RBM15 with CBR3-AS1 as estimated using RNA–protein interaction prediction. **G** Representative immunohistochemistry images of the RBM15 protein in radioresistant and radiosensitive NSCLC samples. **H** Box plot of RBM15 expression in radioresistant and radiosensitive NSCLC patients. The difference was estimated by Wilcoxon rank-sum test. **I** Sankey diagram showing the flow/change of high- and low-RBM15 protein levels in radioresistant and radiosensitive NSCLC samples. **J**–**K** Kaplan–Meier survival curves of 133 NSCLC tumor specimens stratified by RBM15 protein levels as detected using immunohistochemistry. The OS difference was estimated by log-rank test, and HR and 95% CIs were calculated using univariate Cox model

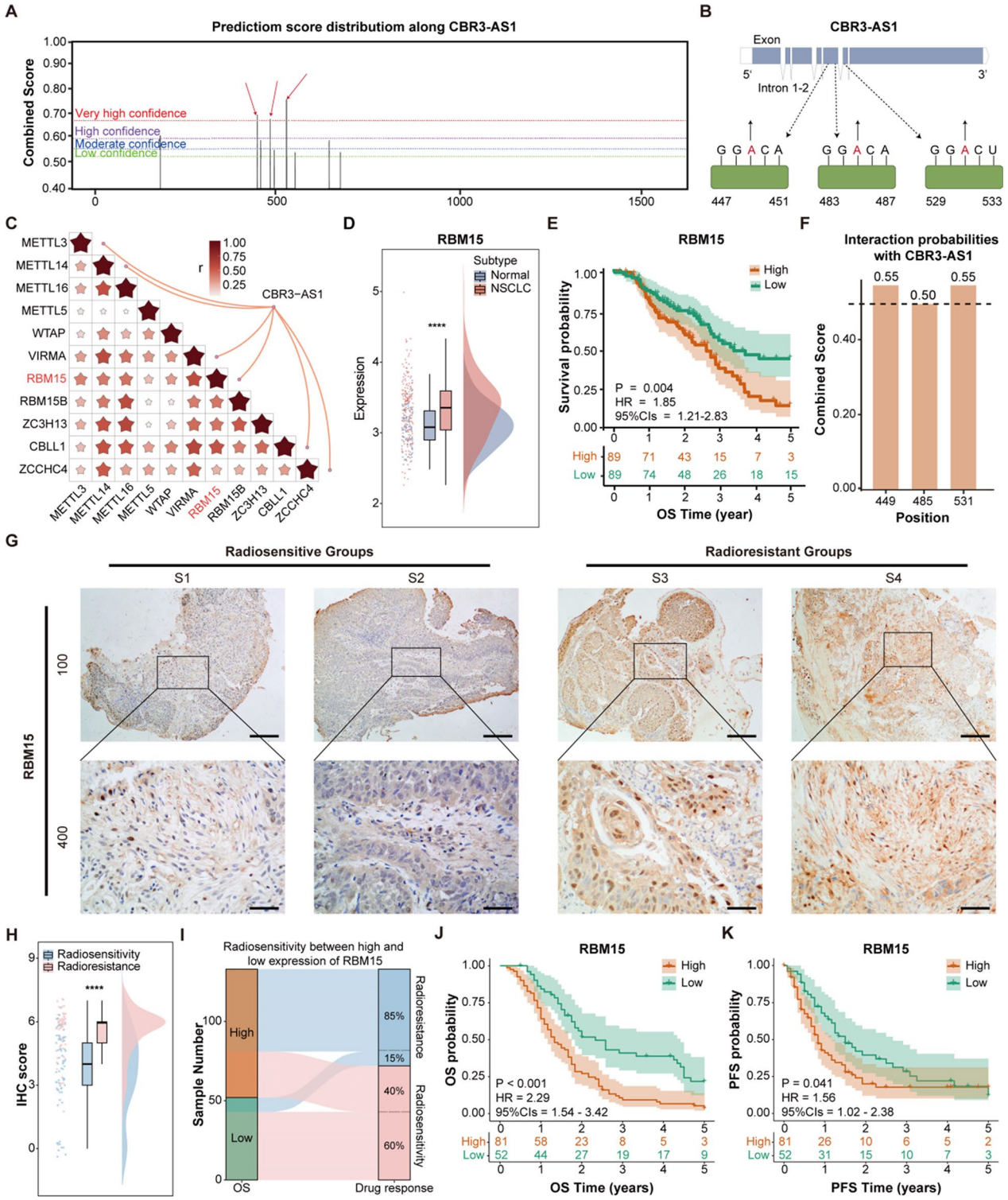

Fig. 1 (See legend on previous page.)

corresponding controls. The results showed that RBM15 overexpression markedly stabilized CBR3-AS1 expression, whereas RBM15 silencing led to a faster decay rate (Fig. 2G). To further investigate whether the m^{6}A modification depended on the m^{6}A residue, we selected the binding site (GGACU) with the highest confidence and constructed wild-type and mutant CBR3-AS1 vectors (CCTGA). The luciferase activity of the construct

Table 1 The association between RBM15 expression and clinicopathological characteristics of NSCLC patients

	RBM15 High Expression (N = 81)	RBM15 Low Expression (N = 52)	Overall (N = 133)	*P*
Gender				
Female	25 (30.9%)	12 (23.1%)	37 (27.8%)	0.428
Male	56 (69.1%)	40 (76.9%)	96 (72.2%)	
Age (year)				
< 60	19(36.5%)	25(30.9%)	44(33.1%)	0.572
> = 60	33(63.5%)	56(69.1%)	89(66.9%)	
Smoke				
Yes	49 (60.5%)	34 (65.4%)	83 (62.4%)	0.715
No	30 (37.0%)	18 (34.6%)	48 (36.1%)	
Missing	2 (2.5%)	0 (0%)	2 (1.5%)	
Alcohol				
Yes	24 (29.6%)	18 (34.6%)	42 (31.6%)	0.571
No	57 (70.4%)	34 (65.4%)	91 (68.4%)	
Stage				
II	1 (1.2%)	0 (0%)	1 (0.8%)	0.578
IIA	4 (4.9%)	4 (7.7%)	8 (6.0%)	
IIB	10 (12.3%)	8 (15.4%)	18 (13.5%)	
III	2 (2.5%)	0 (0%)	2 (1.5%)	
IIIA	36 (44.4%)	18 (34.6%)	54 (40.6%)	
IIIB	23 (28.4%)	15 (28.8%)	38 (28.6%)	
IIIC	5 (6.2%)	7 (13.5%)	12 (9.0%)	
N				
N0	19 (23.5%)	8 (15.4%)	27 (20.3%)	0.379
N1	6 (7.4%)	8 (15.4%)	14 (10.5%)	
N2	39 (48.1%)	24 (46.2%)	63 (47.4%)	
N3	17 (21.0%)	12 (23.1%)	29 (21.8%)	
T				
T1	10 (12.3%)	8 (15.4%)	18 (13.5%)	0.189
T2	39 (48.1%)	23 (44.2%)	62 (46.6%)	
T3	9 (11.1%)	12 (23.1%)	21 (15.8%)	
T4	21 (25.9%)	8 (15.4%)	29 (21.8%)	
Missing	2 (2.5%)	1 (1.9%)	3 (2.3%)	
RECIST1.1				
CR	1 (1.2%)	2 (3.8%)	3 (2.3%)	< 0.001
PD	15 (18.5%)	2 (3.8%)	17 (12.8%)	
PR	31 (38.3%)	40 (76.9%)	71 (53.4%)	
SD	34 (42.0%)	8 (15.4%)	42 (31.6%)	
Chemotherapy				
Gemcitabine + Cisplatin	10 (12.3%)	14 (26.9%)	24 (18.0%)	0.377
Paclitaxel (single agent)	6 (7.4%)	3 (5.8%)	9 (6.8%)	
Paclitaxel + Cisplatin	4 (4.9%)	4 (7.7%)	8 (6.0%)	
Docetaxel + Carboplatin	4 (4.9%)	2 (3.8%)	6 (4.5%)	
Docetaxel + Cisplatin	4 (4.9%)	1 (1.9%)	5 (3.8%)	
Others*	19 (23.5%)	10 (19.2%)	29 (21.8%)	
NO	34 (42.0%)	17 (32.7%)	51 (38.3%)	
Missing	0 (0%)	1 (1.9%)	1 (0.8%)	
Radiotherapy				
Radio sensitivity	29 (35.8%)	43 (82.7%)	72 (54.1%)	< 0.001
Radio resistance	52 (64.2%)	9 (17.3%)	61 (45.9%)	

Table 1 (continued)

* Others Chemotherapy included a total of 16 regimens, such as Docetaxel + Nedaplatin, Paclitaxel + Carboplatin, and Cisplatin + Fluorouracil

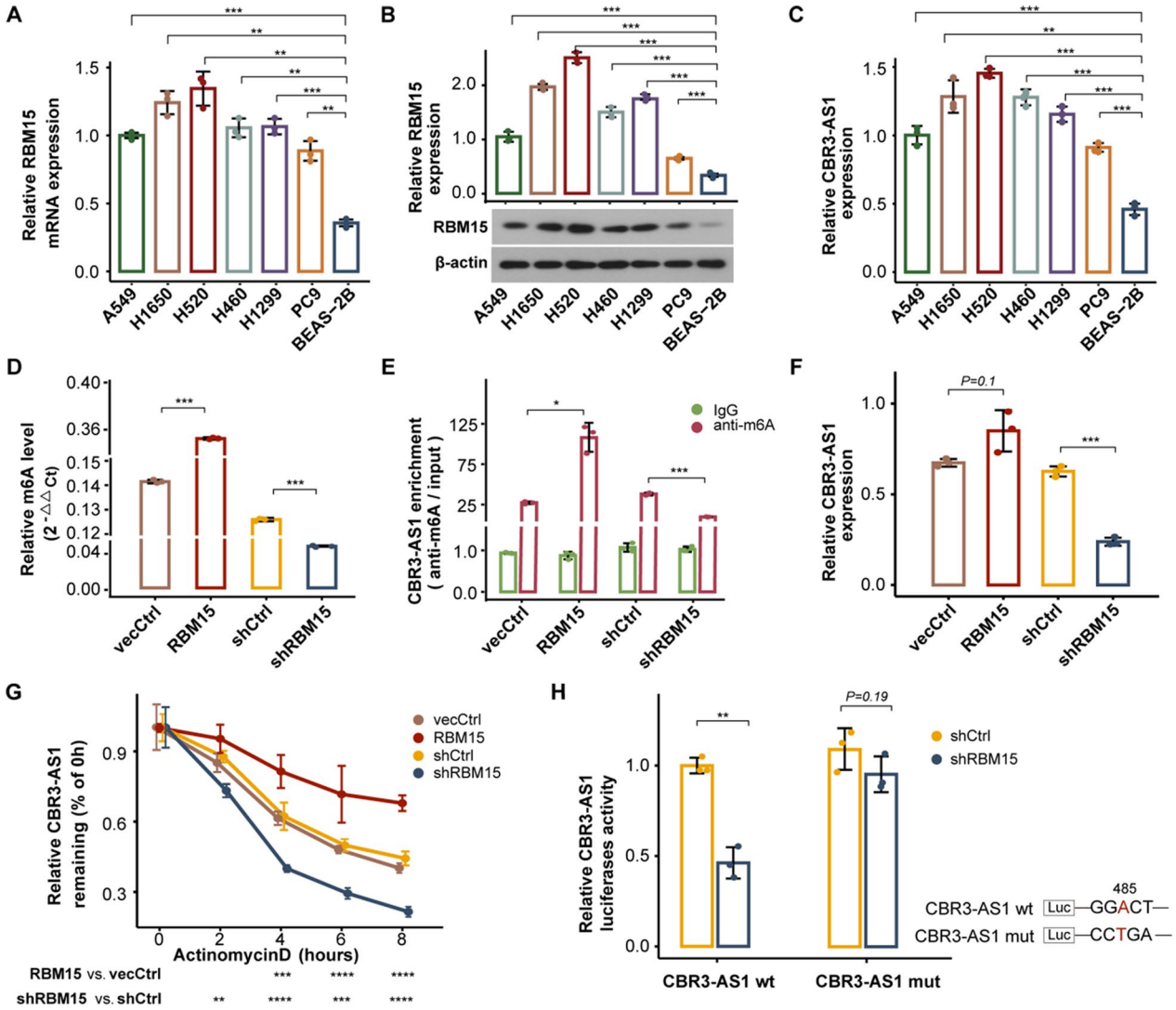

Fig. 2 RBM15 mediates the m^{6}A modification of the lncRNA CBR3-AS1 and promotes its overexpression. **A** Relative mRNA expression of RBM15 in NSCLC cell lines and normal bronchial epithelial cells. **B** Relative protein expression of RBM15 in different lung cell lines and normal bronchial epithelial cells. **C** Relative expression of CBR3-AS1 in different lung cell lines and normal bronchial epithelial cells. **D** Global m^{6}A modification levels in H520 cells. H520 cells were transfected with empty vector control (vecCtrl), RBM15 overexpression plasmid (RBM15), interference control (shCtrl), or specific interference hairpin RNAs targeting RBM15 (shRBM15) and treated with radiation. **E** m.^{6}A methylation levels of CBR3-AS1 in H520 cells as determined using MeRIP-qPCR assays. The input RNA fraction Ct value was used to account for differences in RNA sample preparation. Negative control groups (IgG) were used to adjust the background fraction. **F** Relative expression of CBR3-AS1 in H520 cells as determined using qRT-PCR. **G** RNA stability of CBR3-AS1 in H520 cells. Cells were treated with 5 μg/mL actinomycin D, and RNA was isolated at 0, 2, 4, 6, or 8 h. The significance at different time points between the two groups was analyzed using a one-way analysis of variance (ANOVA). (H) Relative luciferase activity of CBR3-AS1 after RBM15 silencing in the wild-type and mutant CBR3-AS1 groups. The significance between two groups was analyzed using Student's t-test. Data are presented as mean ± standard deviation (mean ± SD) from three independent experiments. Statistical significance was defined as *P < 0.05, **P < 0.01, and ***P < 0.001

containing wild-type CBR3-AS1 decreased significantly upon RBM15 silencing, whereas the luciferase activity of the mutant CBR3-AS1 was unaffected (Fig. 2H).

To ascertain the impact of RBM15 expression on the radioresistance of NSCLC cells, we performed a cell proliferation assay (CCK8), colony formation assay, Transwell invasion assay, wound healing assay, as well as flow cytometry detection of apoptosis in radiation-treated H520 cells. The results showed that RBM15 overexpression significantly abrogated the inhibitory effect of radiation on the viability, proliferation, and invasive capacity of H520 cells, whereas RBM15 silencing enhanced this effect (Fig. 3A–D, Supplementary Fig.S1C–S1E). RBM15 overexpression significantly weakened radiation-induced apoptosis, whereas RBM15 silencing enhanced radiation-induced apoptosis (Fig. 3E).

Previous research has shown that the RBM15-mediated m^6A modification of RNA could be recognized by IGF2BP3, an m^6A reader [13]. Therefore, we speculated that RBM15-mediated m^6A modification enhances the stability of CBR3-AS1 in an IGF2BP3-dependent manner. To verify this inference, we first estimated the interaction probabilities between IGF2BP3 and CBR3-AS1 using RNA–protein interaction prediction (RPISeq, http://pridb.gdcb.iastate.edu/RPISeq/index.html). We found that IGF2BP3 had high interaction probabilities with the three m^6A site sequence motifs of CBR3-AS1 (position: 449, 0.80; position: 485, 0.65; position: 531, 0.5). An RIP assay confirmed that the high-affinity site of CBR3-AS1 was markedly enriched with anti-IGF2BP3 antibodies in H520 cells (Supplementary Fig. S2A).

To clarify the impact of IGF2BP3 on the stability of CBR3-AS1 and radioresistance of NSCLC cells, we established stable H520-IGF2BP3 and H520-shIGF2BP3 cells and the corresponding control H520 cells (vecCtrl and shCtrl). Radiation treatment (8 Gy) was administered 24 h later. IGF2BP3 expression levels were verified (Supplementary Fig. S2B, S2C). IGF2BP3 overexpression increased CBR3-AS1 expression and decreased the rate of CBR3-AS1 degradation, whereas IGF2BP3 silencing decreased CBR3-AS1 expression and accelerated CBR3-AS1 degradation (Supplementary Fig. S2D, S2E). Moreover, silencing IGF2BP3 reduced the luciferase activity of CBR3-AS1 in the CBR3-AS1 wild-type but not in the CBR3-AS1 mutation group (Supplementary Fig. S2F). These results revealed that IGF2BP3 affected the stability of CBR3-AS1. A rescue experiment was conducted to ascertain whether RBM15 and IGF2BP3 are involved in regulating the expression of CBR3-AS1. The expression of CBR3-AS1 was significantly reduced in H520 cells subjected to the simultaneous silencing of RBM15 and IGF2BP3 (Supplementary Fig. S2G). By contrast, the simultaneous overexpression of RBM15 and IGF2BP3 increased CBR3-AS1 expression; the downregulation of RBM15 or IGF2BP3 weakened the upregulation of CBR3-AS1 caused by the overexpression of either protein (Supplementary Fig. S2G).

Cellular experiments showed that the inhibitory effects of radiation on the cell viability, proliferation, and invasion capacities of H520 cells were attenuated by the overexpression of IGF2BP3, while IGF2BP3 silencing enhanced them (Fig. 3F–I, Supplementary Fig. S2H-J). Furthermore, IGF2BP3 overexpression inhibited the radiation-induced apoptosis of H520 cells, whereas the opposite effect was observed after IGF2BP3 silencing (Fig. 3J). Another rescue experiment was conducted to confirm that the IGF2BP3-mediated radioresistance of NSCLC cells was dependent on CBR3-AS1. The results showed that the enhanced effect of radiation on the inhibition of cell proliferation and invasion and promotion of apoptosis in H520 cells induced by IGF2BP3 silencing was abrogated by co-transfection with CBR3-AS1 (Fig. 3K–O, Supplementary Fig. S3A-C).

CBR3-AS1 recruits myeloid suppressor cells (MDSCs) through the miR-409-3p/CXCL1/CXCR2 axis

Our previous research showed that miR-409-3p is a mutually antagonistic RNA to CBR3-AS1, which mediates the CBR3-AS1-induced promotion of radioresistance in NSCLC [4]. To investigate the underlying mechanisms,

(See figure on next page.)

Fig. 3 RBM15 promotes radioresistance in NSCLC. **A** Cell proliferation assay (CCK8) of H520 cells. H520 cells were transfected with an empty vector control (vecCtrl), RBM15 overexpression plasmid (RBM15), interference control (shCtrl), or specific interference hairpin RNAs targeting RBM15 (shRBM15) and treated with radiation. **B** Colony formation assay results of H520 cells transfected with various RBM15 vectors and treated with radiation. **C** Transwell invasion assay of irradiated H520 cells transfected with various RBM15 vectors. **D** Scratch wound healing in irradiated H520 cells at 0 and 24 h, showing cell migration as the % relative to the control. **E** Flow cytometric analysis of cell apoptosis as measured using FITC-annexin V and propidium iodide (PI) staining in H520 cells transfected with various RBM15 vectors and treated with radiation. **F**–**J** CCK8, colony formation, Transwell invasion, and wound healing assays, as well as flow cytometric analysis of H520 cells transfected with vecCtrl, IGF2BP3, shCtrl, or shIGF2BP3, and treated with radiation. **K**–**O** CCK8, colony formation, Transwell invasion, and wound healing assays, as well as flow cytometric analysis of H520 cells transfected with vecCtrl plus shCtrl, CBR3-AS1, shIGF2BP3, or CBR3-AS1 plus shIGF2BP3, and treated with radiation. The significance between two groups was analyzed using Student's t-test. Data are presented as mean ± SD from three independent experiments. Statistical significance was defined as $^*P < 0.05$, $^{**}P < 0.01$, and $^{***}P < 0.001$

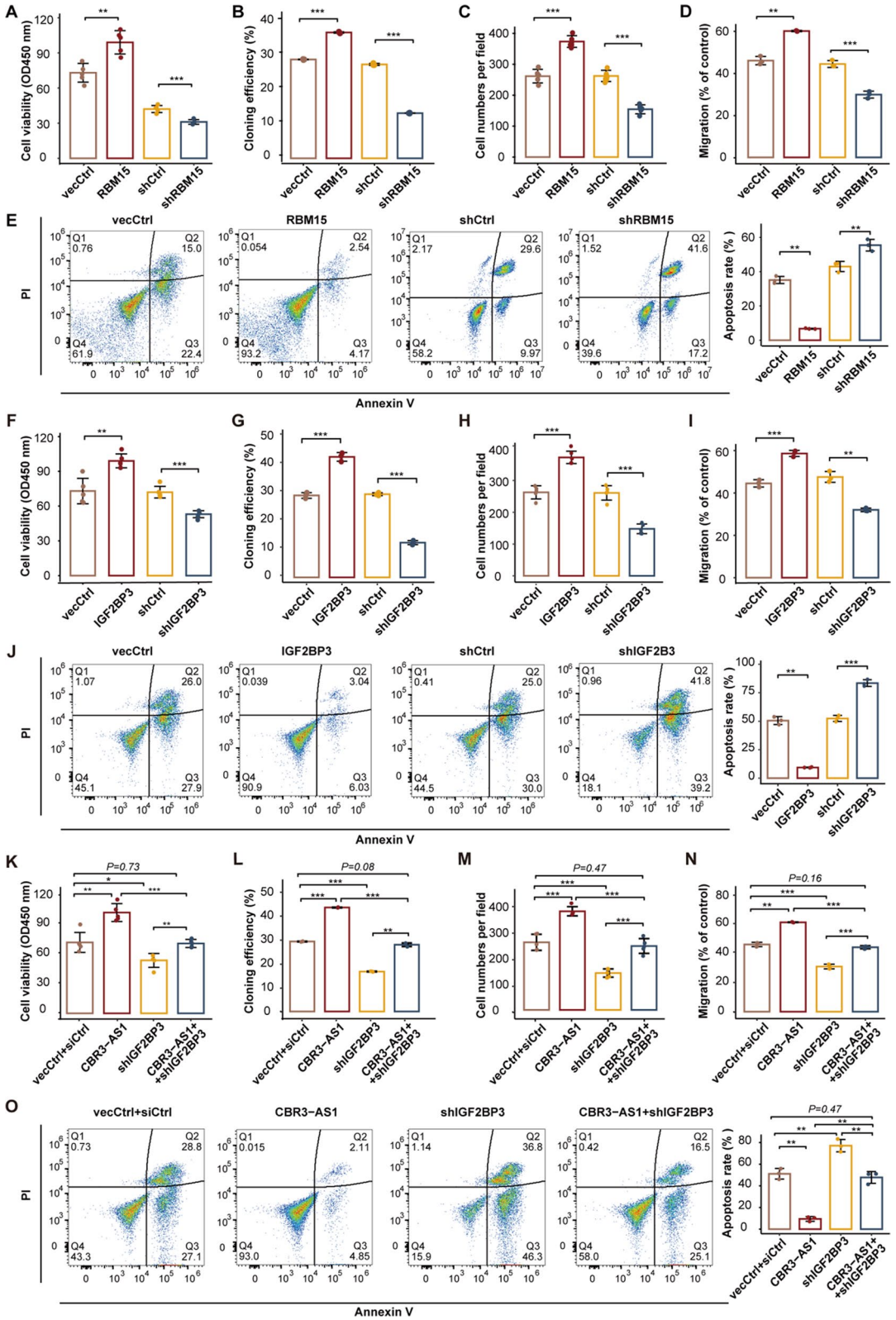

Fig. 3 (See legend on previous page.)

we determined the predicted target genes of miR-409-3p from TargetScan database (https://www.targetscan.org/vert_80/) and focused on CXCL1. CXCL1 could recruit MDSCs into the tumor microenvironment by binding to its receptor CXCR2, thereby inhibiting antitumor immunity and promoting tumor radioresistance [15, 22–24]. Hence, we hypothesized that CBR3-AS1 functions as a competitive endogenous RNA (ceRNA) to regulate CXCL1 expression via miR-409-3p, thereby promoting MDSC recruitment and mediating NSCLC radioresistance. We constructed miR-409-3p overexpressed and silenced lentiviral vectors to infect H520 cells. The cells were then irradiated (8 Gy) after 24 h, and the expression of miR-409-3p was verified via real-time PCR (Supplementary Fig. S4A). As expected, the mRNA and protein expression of CXCL1 was the lowest in the miR-409-3p mimic group and the highest in the miR-409-3p silencing group (Fig. 4A, B). We then used the online tool TargetScan to predict the binding site of CXCL1 targeted by miR-409-3p (Supplementary Fig. S4B) and in cells co-transfected with the wild-type and mutant CXCL1 vectors as well as the miR-409-3p mimic. The results showed that the overexpression of miR-409-3p significantly reduced the luciferase activity of CXCL1 in the wild-type group but not in the mutant group (Fig. 4C). To determine whether CBR3-AS1 influences CXCL1 expression via miR-409-3p, a rescue experiment was performed, and demonstrated that the CBR3-AS1 silencing-induced reductions in the mRNA and protein expression of CXCL1 were reversed by the ablation of miR-409-3p (Fig. 4D, E).

We also assessed the role of CXCL1 in MDSC chemotaxis using an in vitro MDSC migration assay. We isolated MDSCs ($CD11b^+Gr\text{-}1^+$) from the spleens of adult female C57BL/6 mice (age: 6–8 weeks) using magnetically activated cell sorting. We then established stable H520-CXCL1 and H520-shCXCL1 cells via lentivirus transfection and the corresponding controls (vecCtrl and shCtrl). The results showed that CXCL1 silencing significantly decreased the migration ability of $CD11b^+Gr\text{-}1^+$ MDSCs toward the conditioned medium of H520 cells, whereas CXCL1 overexpression significantly increased the migration ability of $CD11b^+Gr\text{-}1^+$ MDSCs (Fig. 4F). By contrast, blockade of the CXCL1 receptor CXCR2 using SB265610 markedly diminished $CD11b^+Gr\text{-}1^+$ MDSC migration mediated by CXCL1 overexpression (Fig. 4F), indicating that the CXCL1-CXCR2 axis promoted $CD11b^+Gr\text{-}1^+$ MDSC migration. To further evaluate the effect of $CD11b^+Gr\text{-}1^+$ MDSCs on the immune response, we sorted $CD8^+$ and $CD4^+$ T cells from the spleens of adult female C57BL/6 mice (age: 6–8 weeks). $CD8^+$ and $CD4^+$ T cells were activated with anti-CD3/CD28-coated Dynabeads and then co-cultured with $CD11b^+Gr\text{-}1^+$ MDSCs derived from the four groups (shCtrl, shCXCL1, vecCtrl, and CXCL1). We found that CXCL1 silencing enhanced the production of interferon (IFN)-γ in tumor-infiltrating $CD8^+$ and $CD4^+$ T cells, whereas CXCL1 overexpression suppressed IFN-γ production (Fig. 4G and H). Moreover, the suppressive effect of $CD11b^+Gr\text{-}1^+$ MDSCs on $CD8^+$ and $CD4^+$ T cells in the CXCL1 group was rescued by SB265610 treatment (Fig. 4G and H).

Finally, we explored the involvement of miR-409-3p and CXCL1 in the mechanism by which CBR3-AS1 promotes radioresistance in NSCLC. The results showed that silencing CBR3-AS1 enhanced the inhibitory effect of radiation on the viability, proliferation, and invasion capacities of H520 cells, whereas this inhibition was attenuated by the knockdown of miR-409-3p (Fig. 5A–D). The strengthened inhibitory effect of radiation on the viability, proliferation, and invasion capacities of NSCLC cells induced by the overexpression of miR-409-3p was reduced after the addition of CXCL1 (Fig. 5A–D). Flow cytometry revealed that CBR3-AS1 silencing enhanced radiation-induced apoptosis, and this enhancement was weakened by silencing miR-409-3p. Similarly, the enhanced radiation-induced apoptosis caused by miR-409-3p overexpression was weakened following CXCL1 overexpression (Fig. 5E).

RBM15 depletion suppresses NSCLC radioresistance in vivo

To confirm the role of RBM15 in promoting NSCLC radioresistance in vivo, we constructed a mouse-derived RBM15-silencing lentivirus and the corresponding negative control to infect mouse lung cancer cells (LCC), and then approximately 2×10^6 LCC (shRBM15) and control cells (shCtrl) were injected into C57BL/6 mice. The mice were then treated with a total of 20 Gy in five fractions of tumor-localized radiation (4 Gy per fraction) or sham treatment (Fig. 6A). Radiation treatment effectively reduced the volume of tumors (Fig. 6B, Supplementary Fig. S5), and its effectiveness was increased by silencing RBM15 (Fig. 6B, Supplementary Fig. S5). Hematoxylin and eosin (HE) staining was performed to identify tumors (Fig. 6C, upper panel). IHC analysis demonstrated a decrease in the proportion of proliferating cell nuclear antigen (PCNA)-stained cells in radiation-treated shRBM15-LLC mice compared to the mice in the other groups (Fig. 6C, middle panel). Moreover, terminal deoxynucleotidyl transferase-mediated deoxyuridine triphosphate nick-end labeling (TUNEL) assay revealed that radiation-treated shRBM15-LCC mice exhibited a greater degree of cell apoptosis than the other mice (Fig. 6C, lower panel).

The expression levels of RBM15, CBR3-AS1, IGF2BP3, CXCL1, and CXCR2 were the lowest in radiation-treated

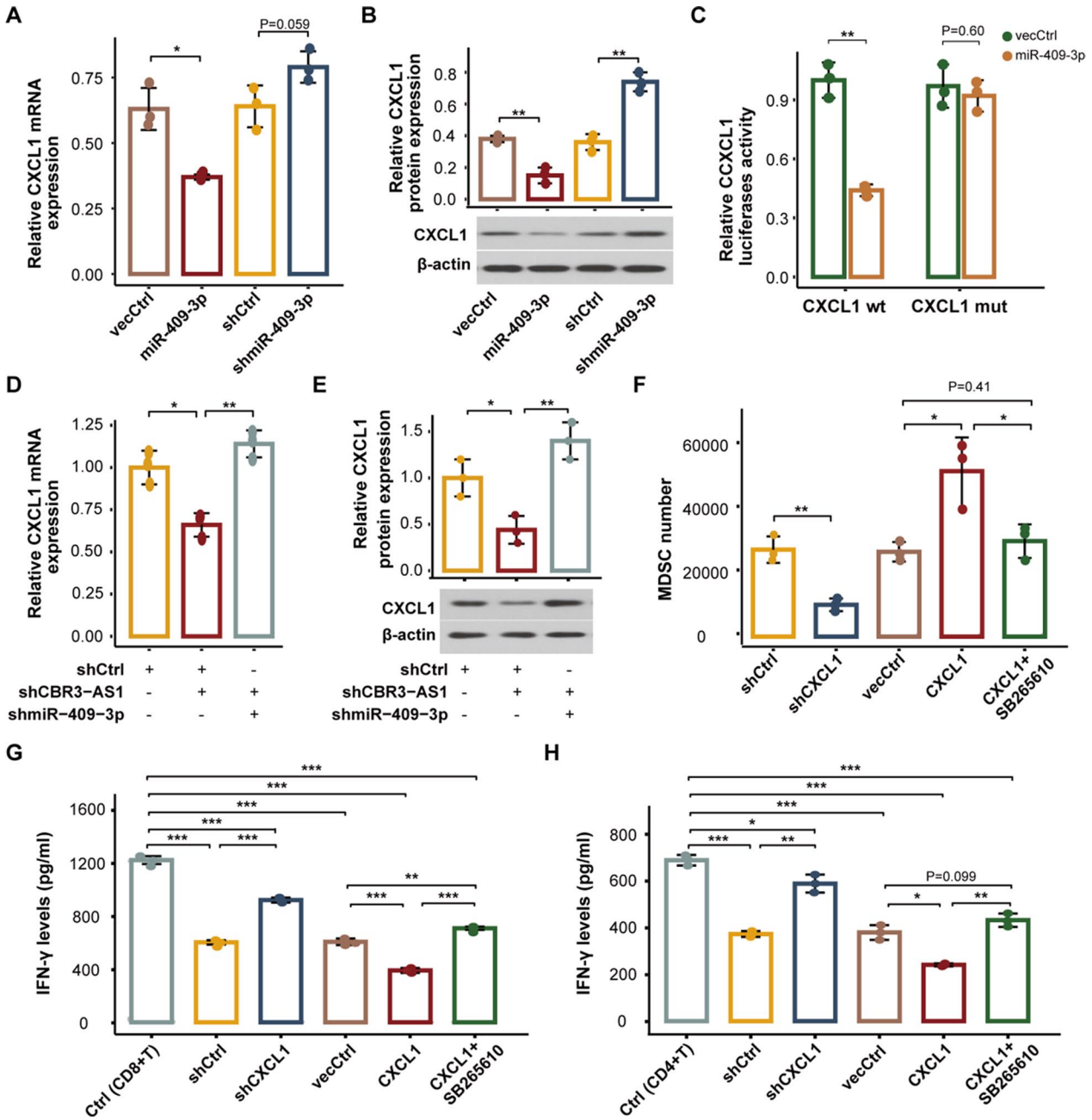

Fig. 4 CBR3-AS1 recruits MDSCs through the miR-409-3p/CXCL1/CXCR2 axis. **A** Relative mRNA expression levels of CXCL1 in H520 cells transfected with a control empty vector (vecCtrl), miR-409-3p mimic plasmid (miR-409-3p), control shRNA (shCtrl), or specific interfering hairpin RNAs targeting miR-409-3p (shmiR-409-3p). The cells were exposed to radiation after 24 h of transfection. **B** Relative protein expression levels of CXCL1 in H520 cells. β-actin was used as the reference for normalization. **C** Relative luciferase activity of CXCL1 under miR-409-3p overexpression in the wild-type and mutant CXCL1 groups treated with radiation. **D**, **E** Relative mRNA and protein expression levels of CXCL1 in H520 cells transfected with shCtrl, shCBR3-AS1, or shmiR-409-3p. **F** Migration ability of MDSCs toward the conditioned medium of H520 cells transfected with CXCL1, shCXCL1, or treated with a CXCR2 inhibitor (SB265610, 10 mM) and treated with radiation. **G**, **H** Levels of interferon (IFN)-γ secreted by $CD8^+$ and $CD4.^+$ T cells co-cultured with H520 cells transfected with CXCL1, shCXCL1 or treated with a CXCR2 inhibitor (SB265610, 10 mM). IFN-γ expression was reported as the mean fluorescence intensity. The significance between two groups was analyzed using Student's t-test. Data are presented as mean ± SD from three independent experiments. Statistical significance was defined as *P < 0.05, **P < 0.01, and ***P < 0.001

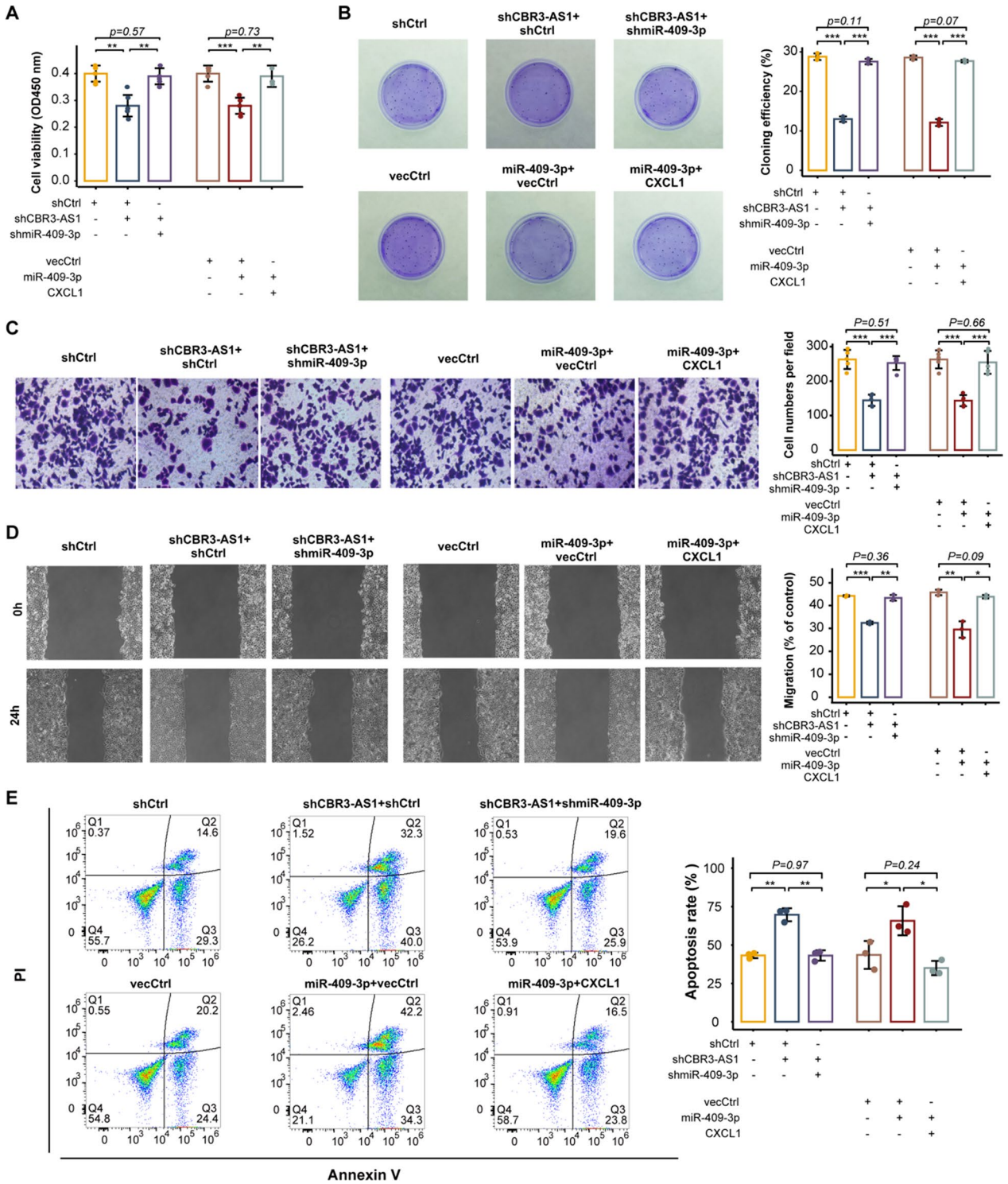

Fig. 5 CBR3-AS1 participates in the radioresistance of H520 cells by regulating the miR-409-3p and CXCL1 axis. **A**, **B** The viability and proliferation of H520 cells were assessed using the CCK8 and colony formation assays, respectively. **C** Invasion ability of H520 cells. **D** Scratch wound healing in H520 cells at 0 and 24 h. **E** Apoptosis levels in H520 cells as assessed via flow cytometry. H520 cells were transfected with shCBR3-AS1, shmiR-409-3p, CBR3-AS1, or miR-409-3p, and then exposed to radiation. The significance between two groups was analyzed using Student's t-test. Data are presented as mean ± SD from three independent experiments. Statistical significance was defined as *P < 0.05, **P < 0.01, and ***P < 0.001

shRBM15-LCC mice, while the expression of miR-409-3p was highest in these mice (Fig. 6D, E). m^6A quantification and MeRIP-qPCR assays using tumor tissues showed a significant reduction in the global m^6A levels and m^6A modification levels of CBR3-AS1 in radiation-treated shRBM15 mice compared with those in the mice from the other groups (Fig. 6F, G).

To further confirm the role of RBM15 in inhibiting the antitumor immune response, we sorted $CD11b^+Gr\text{-}1^+$ MDSCs and $CD8^+$ and $CD4^+$ T cells from the tumor tissues of LCC tumor-bearing mice (age: 4–6 weeks). Flow cytometry analysis demonstrated a pronounced reduction in the percentage of MDSCs and an increase in the percentage of $CD8^+$ and $CD4^+$ T cells in tumors derived from radiation-treated shRBM15-LCC mice (Fig. 6H, I). Furthermore, we observed an increased number of IFN-γ-producing $CD8^+$ and $CD4^+$ T cells in radiation-treated shRBM15 allografts, suggesting enhanced T cell activation (Fig. 6J).

Discussion

Radiotherapy is a common treatment for NSCLC, however, radioresistance greatly limits the clinical efficacy and prognosis of patients with cancer and remains an intractable challenge. The lncRNA CBR3-AS1 CBR3-AS1 has been reported to be involved in tumorigenesis and the progression of various cancers [25]. Our previous study found that CBR3-AS1 mediates radioresistance in NSCLC by sponging miR-409-3p [4], however, the radioresistance mechanism underlying CBR3-AS1 remains unclear. In the present study, our data revealed that the methyltransferase RBM15 induces CBR3-AS1 overexpression via an m^6A-IGF2BP3-dependent mechanism, which subsequently induces CXCL1 overexpression by sponging miR-409-3p to recruit MDSCs and inhibit T cell activity, thereby facilitating NSCLC radioresistance.

m^6A is the most common epigenetic modification of RNA, and it is associated with various human cancers [8, 9]. In this study, we found that the m^6A site was highly enriched within CBR3-AS1, indicating that m^6A modifications may facilitate CBR3-AS1 overexpression in NSCLC. Transcriptomic analyses of NSCLC samples indicated that RBM15 is a methyltransferase that mediates the m^6A modification of CBR3-AS1 and promotes its overexpression, as confirmed via real time PCR, MeRIP-qPCR and luciferase reporter assays in vitro.

RBM15, a member of the SPEN (split-end) family of proteins, recruits methyltransferase complexes and regulates m^6A modification by binding to its target RNAs [26]. A previous study has shown that RBM15 can accelerate progression and metastasis by mediating m^6A methylation in multiple cancers, such as laryngeal squamous cell carcinoma [13], colorectal cancer [27], cervical cancer [28], and glioma [29]. However, the role of RBM15 in radioresistance has not been thoroughly clarified. In the present study, our data revealed that RBM15 overexpression enhanced the effect of radiation on inhibiting the proliferation and invasion and promoting the apoptosis of NSCLC cells. RBM15 silencing weakened this effect. Clinical samples also validated the correlation of RBM15 with the radiosensitivity and prognosis of patients with NSCLC receiving radiotherapy. Collectively, these results indicate that RBM15 plays a non-negligible role in NSCLC radioresistance by mediating the m^6A modification of CBR3-AS1 and could be a potential biomarker and therapeutic target in NSCLC.

m^6A "readers" are considered regulators of mRNA metabolism, and the IGF2BP family is associated with the stability of methylated RNA [30]. The role of IGF2BP3 in tumor occurrence and progression is well-characterized [31, 32]. Previous studies have shown that RBM15 facilitates tumor proliferation and metastasis by enhancing mRNA stability in an IGF2BP3-dependent manner [13, 27]. Therefore, this study investigated whether IGF2BP3 is responsible for the stability of m^6A-modified CBR3-AS1 mediated by RBM15. Molecular docking analysis

(See figure on next page.)

Fig. 6 RBM15 depletion suppresses NSCLC radioresistance in vivo. **A** Schematic diagram of lung cancer cell (LCC)-bearing C57BL/6 mice. The mice were randomly divided into two groups and injected with shRBM15-LCC or shCtrl-LCC. When the tumor volume reached approximately 200 mm^3, the mice in each group were randomly divided into two groups and treated with a total of 20 Gy in five fractions via tumor-localized radiation (radiation-treated shRBM15 or radiation-treated shCtrl mice) or sham treatment. **B** Tumor growth and volume in tumor-bearing C57BL/6 mice with or without RBM15 knockdown and subjected to radiation or sham treatment. The significance at different time points between the two groups was analyzed using ANOVA. **C** Representative images of HE staining (upper panel), immunohistochemistry (IHC) staining with antibodies against PCNA (middle panel), and TUNEL assays showing apoptosis in tumor-bearing LCC mice (lower panel). **D** Relative RNA expression levels of RBM15, CBR3-AS1, IGF2BP3, miR-409-3p, CXCL1, and CXCR2 in H520 tumor-bearing C57BL/6 mice. **E** Relative protein expression levels of RBM15, IGF2BP3, CXCL1, and CXCR2 in LCC tumor-bearing C57BL/6 mice. **F** Global levels of m^6A modifications in tumor-bearing LCC mice. **G** m^6A methylation levels in CBR3-AS1 in tumor-bearing LCC mice. (H) Percentages of myeloid-derived suppressor cells (MDSCs) in tumor-bearing LCC mice. **I** Percentages of $CD8^+$ and $CD4^+$ T cells in tumor-bearing LCC mice. **J** Percentages of IFN-γ-producing $CD8^+$ and $CD4.^+$ T cells in tumor-bearing LCC mice. The significance between two groups was analyzed using Student's t-test. Data are presented as mean ± SD from three independent experiments. Statistical significance was defined as $^*P < 0.05$, $^{**}P < 0.01$, and $^{***}P < 0.001$

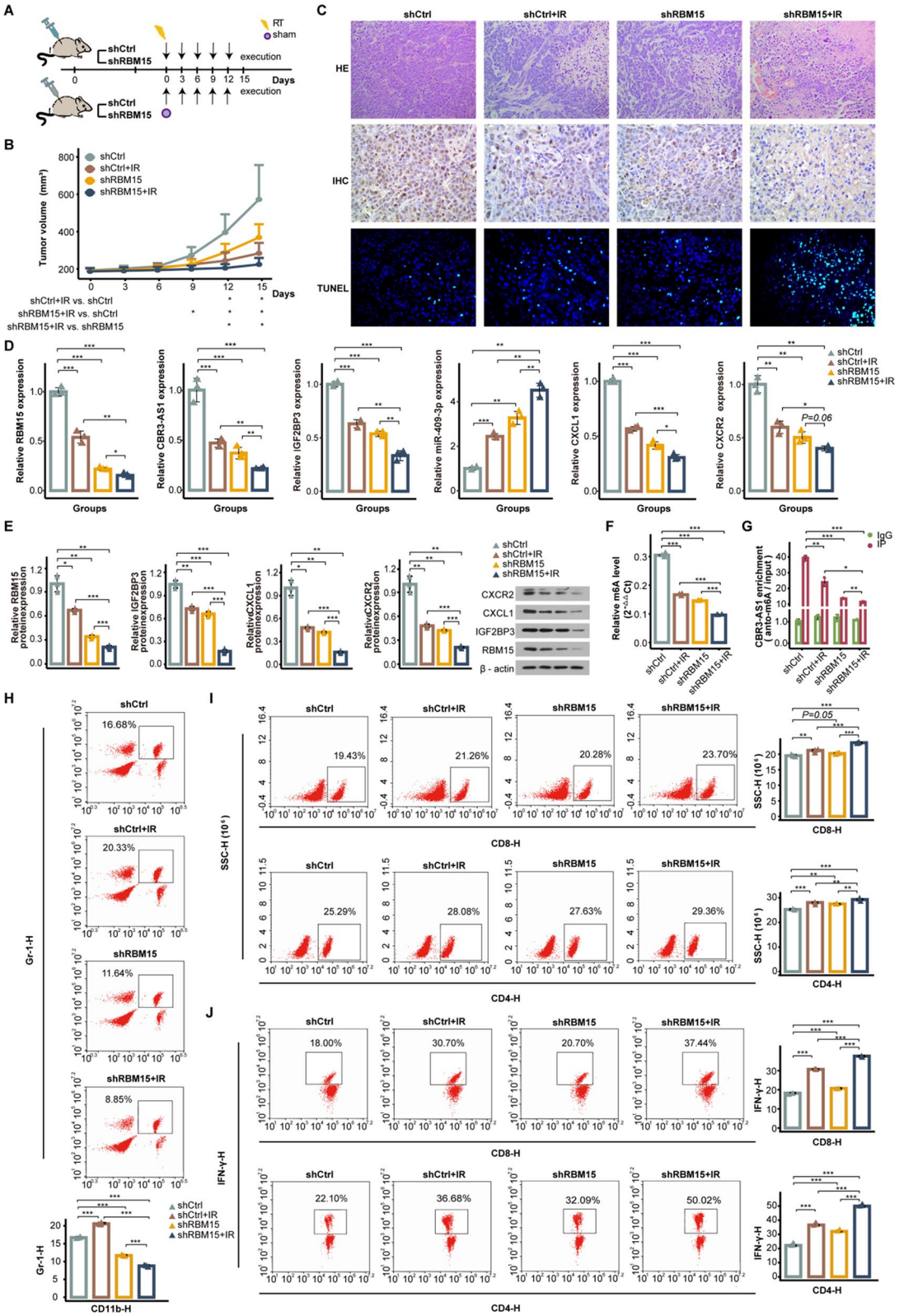

Fig. 6 (See legend on previous page.)

showed that IGF2BP3 could bind to the m^{6}A sites of CBR3-AS1. Real time PCR, RIP, and luciferase reporter assays in NSCLC cell lines confirmed that IGF2BP3 enhanced the expression and stability of CBR3-AS1. Cell experiments demonstrated that IGF2BP3 overexpression attenuated the effects of radiation on cell survival and invasion. By contrast, IGF2BP3 silencing enhanced the inhibitory effects of radiation on NSCLC cells, and this enhancement could be abrogated by overexpressing CBR3-AS1. Our data indicate that the m^{6}A reader IGF2BP3 interprets the RBM15-mediated m^{6}A modification of CBR3-AS1 and maintains its stability by preventing its degradation, promoting radioresistance in NSCLC.

The accumulation of MDSCs in the tumor microenvironment can inhibit the antitumor activity of T cells and contribute to radioresistance [14]. We inferred that CBR3-AS1 functions as a ceRNA to regulate CXCL1 expression, a target of miR-409-3p, and mediates radioresistance by recruiting MDSCs. Using real-time PCR, western blot, and luciferase reporter assays, we demonstrated CXCL1 as a target of miR-409-3p. Moreover, the overexpression of miR-409-3p inhibited CXCL1 expression, while the miR-409-3p silencing had the opposite effect. Rescue experiments showed that silencing CBR3-AS1 decreased CXCL1 expression, and this effect could be reversed by silencing miR-409-3p. Our study further revealed that CXCL1 drives MDSC accumulation and suppresses T cell activity, and these effects are abrogated after CXCL1 silencing or administering a CXCR2 inhibitor. Further rescue experiments demonstrated that the enhanced inhibitory effect of radiation on NSCLC cells induced by CBR3-AS1 silencing was abrogated by miR-409-3p knockdown. Similarly, the enhanced inhibitory effect of radiation on NSCLC cells induced by miR-409-3p overexpression was suppressed by CXCL1 overexpression. These results collectively support our inference that CBR3-AS1 induces the miR-409-3p-CXCL1/CXCR2 axis to recruit MDSCs and inhibit T activity, promoting radioresistance in NSCLC.

Consistent with the in vitro observations, mouse xenograft models showed that the inhibitory effect of radiation on tumor cells was significantly enhanced when RBM15-silenced LCCs were injected intravenously into mice. We also confirmed that RBM15 silencing inhibited the global m^{6}A and m^{6}A modification levels of CBR3-AS1 and influenced the expression of IGF2BP3, miR-409-3p, CXCL1, and CXCR2. As expected, the depletion of RBM15 in NSCLC cells remarkably reduced MDSC accumulation in tumors and enhanced the antitumor activity of T cells.

This study has some limitations. First, according to the current treatment guidelines, stage II–III unresectable NSCLC needs to be treated using chemoradiotherapy, the clinical samples in this study may have included some patients who have undergone concurrent chemoradiotherapy. Hence, the effect of chemotherapy on radiosensitivity was not discussed in this study. Secondly, our results indicate that the RBM15/IGF2BP3/CBR3-AS1/miR-409-3p/CXCL1 axis might inhibit the efficacy of anti-PD-1 or anti-PD-L1 immunotherapy in NSCLC by recruiting MDSC aggregation to inhibit antitumor activity of T cells, thus experiments are in progress to explore this avenue. Thirdly, the lack of inhibitors targeting RBM15 and other genes in the axis limits the clinical translation. Therefore, in the follow-up study, we are planning to design a small-molecule inhibitor of RBM15 and explore new delivery modes, such as nanoparticles, to effectively demonstrate its clinical potential in radiosensitizing radiotherapy of NSCLC patients. In addition, whether there are other m^{6}A methyltransferases that have a regulatory role in this signaling pathway remains unknown and should be investigated.

Conclusion

In conclusion, we demonstrated the role and mechanism of how the methyltransferase RBM15 mediates radioresistance in NSCLC. Mechanistically, RBM15 activates the m^{6}A- IGF2BP3/CBR3-AS1/miR-409-3p/CXCL1 axis to recruit MDSCs and inhibit T cell activity, promoting NSCLC radioresistance. Moreover, the depletion of RBM15 enhances the tumor-inhibiting effect of radiation on NSCLC, highlighting RBM15 as a potential target for radiosensitization in NSCLC.

Supplementary Information

The online version contains supplementary material available at https://doi.org/10.1186/s12967-025-06205-y.

Additional file 1.

Acknowledgements

We wish to thank all participants and investigators for their participation of the study.

Author contributions

SLH, NZ, and JL performed the study and wrote the manuscript. SLL, LSQ, SLH, and NZ helped in most of the experiments. JL, LQW, and LSQ contributed to verifying the results and revising the manuscript. KJ, YXW, YCW, YYC, and YB participated in checking the medical records. JXZ, YYL, and LSQ contributed to the statistical analysis. All authors read the manuscript and approved the final version.

Funding

This work was supported by the Hai Yan Fund of The Third Affiliated Hospital of Harbin Medical University, Harbin, China (JJZD2023-01) to SLL, project under the guidance of Xiamen Health Care (3502Z2014ZD1142) to NZ, the Young Investigator Research Program of Xiang'an Hospital of Xiamen

University (XM01320001) to NZ, and the Outstanding Youth Foundation of Heilongjiang Province of China (No. YQ2023H002) to LSQ.

Availability of data and materials

The public data analyzed in this study were obtained from The Cancer Genome Atlas (TCGA) datasets, specifically the LUAD dataset and the LUSC dataset. All the data used or analyzed in this study are included in this article.

Declarations

Ethics approval and consent to participate

All human tumor tissue samples were collected in accordance with national and in-stitutional ethical guidelines. The protocol employed in this study was approved by the Medical Ethics Committee (KY2022-57). All patients have signed informed consent forms. All animal studies (including the mice euthanasia procedure) complied with the regulations and guidelines of Harbin Medical University institutional animal care (JJZD 2023-01) and conducted according to The American Association for Laboratory Animal Science and the Institutional Animal Care and Use Committee guidelines.

Consent for publication

Not applicable.

Competing interests

The authors declare that they have no competing interests.

Author details

[1]Department of Thoracic Radiation Oncology, Harbin Medical University Cancer Hospital, Harbin, China. [2]Department of Radiation Oncology, Xiang'an Hospital of Xiamen University, Xiamen, China. [3]College of Bioinformatics Science and Technology, Harbin Medical University, Harbin, China.

Received: 25 October 2024 Accepted: 5 February 2025
Published online: 17 February 2025

References

1. Siegel RL, Giaquinto AN, Jemal A. Cancer statistics, 2024. CA Cancer J Clin. 2024;74(1):12–49. https://doi.org/10.3322/caac.21820.
2. Ettinger DS, Wood DE, Aisner DL, Akerley W, Bauman JR, Bharat A, et al. NCCN guidelines(R) insights: non-small cell lung cancer, version 2.2023. J Natl Compr Canc Netw. 2023;21(4):340–50. https://doi.org/10.6004/jnccn.2023.0020.
3. Vinod SK. International patterns of radiotherapy practice for non-small cell lung cancer. Semin Radiat Oncol. 2015;25(2):143–50. https://doi.org/10.1016/j.semradonc.2014.11.001.
4. Liu S, Zhan N, Gao C, Xu P, Wang H, Wang S, et al. Long noncoding RNA CBR3-AS1 mediates tumorigenesis and radiosensitivity of non-small cell lung cancer through redox and DNA repair by CBR3-AS1 /miR-409–3p/SOD1 axis. Cancer Lett. 2022;526:1–11. https://doi.org/10.1016/j.canlet.2021.11.009.
5. Hou M, Wu N, Yao L. LncRNA CBR3-AS1 potentiates Wnt/beta-catenin signaling to regulate lung adenocarcinoma cells proliferation, migration and invasion. Cancer Cell Int. 2021;21(1):36. https://doi.org/10.1186/s12935-020-01685-y.
6. Yao W, Hou J, Liu G, Wu F, Yan Q, Guo L, et al. LncRNA CBR3-AS1 promotes osteosarcoma progression through the network of miR-140–5p/DDX54-NUCKS1-mTOR signaling pathway. Mol Ther Oncolytics. 2022;25:189–200. https://doi.org/10.1016/j.omto.2022.03.001.
7. Zhang M, Wang Y, Jiang L, Song X, Zheng A, Gao H, et al. LncRNA CBR3-AS1 regulates of breast cancer drug sensitivity as a competing endogenous RNA through the JNK1/MEK4-mediated MAPK signal pathway. J Exp Clin Cancer Res. 2021;40(1):41. https://doi.org/10.1186/s13046-021-01844-7.
8. Frye M, Harada BT, Behm M, He C. RNA modifications modulate gene expression during development. Science. 2018;361(6409):1346–9. https://doi.org/10.1126/science.aau1646.
9. Meyer KD, Jaffrey SR. The dynamic epitranscriptome: N6-methyladenosine and gene expression control. Nat Rev Mol Cell Biol. 2014;15(5):313–26. https://doi.org/10.1038/nrm3785.
10. Roundtree IA, Evans ME, Pan T, He C. Dynamic RNA modifications in gene expression regulation. Cell. 2017;169(7):1187–200. https://doi.org/10.1016/j.cell.2017.05.045.
11. Fang H, Sun Q, Zhou J, Zhang H, Song Q, Zhang H, et al. m(6)A methylation reader IGF2BP2 activates endothelial cells to promote angiogenesis and metastasis of lung adenocarcinoma. Mol Cancer. 2023;22(1):99. https://doi.org/10.1186/s12943-023-01791-1.
12. Wang L, Dou X, Chen S, Yu X, Huang X, Zhang L, et al. YTHDF2 inhibition potentiates radiotherapy antitumor efficacy. Cancer Cell. 2023;41(7):1294–308. https://doi.org/10.1016/j.ccell.2023.04.019.
13. Wang X, Tian L, Li Y, Wang J, Yan B, Yang L, et al. RBM15 facilitates laryngeal squamous cell carcinoma progression by regulating TMBIM6 stability through IGF2BP3 dependent. J Exp Clin Cancer Res. 2021;40(1):80. https://doi.org/10.1186/s13046-021-01871-4.
14. Liang H, Deng L, Hou Y, Meng X, Huang X, Rao E, et al. Host STING-dependent MDSC mobilization drives extrinsic radiation resistance. Nat Commun. 2017;8(1):1736. https://doi.org/10.1038/s41467-017-01566-5.
15. Zhou X, Fang D, Liu H, Ou X, Zhang C, Zhao Z, et al. PMN-MDSCs accumulation induced by CXCL1 promotes CD8(+) T cells exhaustion in gastric cancer. Cancer Lett. 2022. https://doi.org/10.1016/j.canlet.2022.215598.
16. Liu S, Li B, Xu J, Hu S, Zhan N, Wang H, et al. SOD1 promotes cell proliferation and metastasis in non-small cell lung cancer via an miR-409–3p/SOD1/SETDB1 epigenetic regulatory feedforward loop. Front Cell Dev Biol. 2020. https://doi.org/10.3389/fcell.2020.00213.
17. Fleet JC, Burcham GN, Calvert RD, Elzey BD, Ratliff TL. 1alpha, 25 Dihydroxyvitamin D (1,25(OH)(2)D) inhibits the T cell suppressive function of myeloid derived suppressor cells (MDSC). J Steroid Biochem Mol Biol. 2020. https://doi.org/10.1016/j.jsbmb.2019.105557.
18. Huang H, Weng H, Chen J. m(6)A modification in coding and non-coding RNAs: Roles and therapeutic implications in cancer. Cancer Cell. 2020;37(3):270–88. https://doi.org/10.1016/j.ccell.2020.02.004.
19. Li Y, Xiao J, Bai J, Tian Y, Qu Y, Chen X, et al. Molecular characterization and clinical relevance of m(6)A regulators across 33 cancer types. Mol Cancer. 2019;18(1):137. https://doi.org/10.1186/s12943-019-1066-3.
20. Liu J, Harada BT, He C. Regulation of gene expression by N(6)-methyladenosine in cancer. Trends Cell Biol. 2019;29(6):487–99. https://doi.org/10.1016/j.tcb.2019.02.008.
21. Nombela P, Miguel-Lopez B, Blanco S. The role of m(6)A, m(5)C and Psi RNA modifications in cancer: novel therapeutic opportunities. Mol Cancer. 2021;20(1):18. https://doi.org/10.1186/s12943-020-01263-w.
22. Bhattarai S, Mackeyev Y, Venkatesulu BP, Krishnan S, Singh PK. CXC chemokine receptor 4 (CXCR4) targeted gold nanoparticles potently enhance radiotherapy outcomes in breast cancer. Nanoscale. 2021;13(45):19056–65. https://doi.org/10.1039/d1nr05385j.
23. Li BH, Garstka MA, Li ZF. Chemokines and their receptors promoting the recruitment of myeloid-derived suppressor cells into the tumor. Mol Immunol. 2020;117:201–15. https://doi.org/10.1016/j.molimm.2019.11.014.
24. Walle T, Kraske JA, Liao B, Lenoir B, Timke C, et al. Radiotherapy orchestrates natural killer cell dependent antitumor immune responses through CXCL8. Sci Adv. 2022;8(12):4050. https://doi.org/10.1126/sciadv.abh4050.
25. Esteller M. Non-coding RNAs in human disease. Nat Rev Genet. 2011;12(12):861–74. https://doi.org/10.1038/nrg3074.
26. Wang T, Kong S, Tao M, Ju S. The potential role of RNA N6-methyladenosine in cancer progression. Mol Cancer. 2020;19(1):88. https://doi.org/10.1186/s12943-020-01204-7.
27. Chen J. Regulatory mechanism of RNA binding motif protein 15-mediated N(6) methyladenosine modification in proliferation, invasion, and migration of colorectal cancer cells. Environ Toxicol. 2023;38(11):2545–59. https://doi.org/10.1002/tox.23883.
28. Song Y, Wu Q. RBM15 m(6) A modification-mediated OTUB2 upregulation promotes cervical cancer progression via the AKT/mTOR signaling. Environ Toxicol. 2023;38(9):2155–64. https://doi.org/10.1002/tox.23852.
29. Guo X, Qiu W, Wang C, Qi Y, Li B, Wang S, et al. Neuronal activity promotes glioma progression by inducing proneural-to-mesenchymal transition in glioma stem cells. Cancer Res. 2024;84(3):372–87. https://doi.org/10.1158/0008-5472.CAN-23-0609.
30. Zhu TY, Hong LL, Ling ZQ. Oncofetal protein IGF2BPs in human cancer: functions, mechanisms and therapeutic potential. Biomark Res. 2023;11(1):62. https://doi.org/10.1186/s40364-023-00499-0.
31. Cui Y, Wu Y, Wang C, Wang Z, Li Y, Jiang Z, et al. Isoliquiritigenin inhibits non-small cell lung cancer progression via m(6)A/IGF2BP3-dependent TWIST1

mRNA stabilization. Phytomedicine. 2022. https://doi.org/10.1016/j.phymed.2022.154299.
32. Zhang X, Chen Q, He Y, Shi Q, Yin C, Xie Y, et al. STRIP2 motivates non-small cell lung cancer progression by modulating the TMBIM6 stability through IGF2BP3 dependent. J Exp Clin Cancer Res. 2023;42(1):19. https://doi.org/10.1186/s13046-022-02573-1.

Publisher's Note